ELSEVIER

Journal of Power Sources 96 (2001) 226–232

JOURNAL OF POWER SOURCES

www.elsevier.com/locate/jpowsour

In situ X-ray absorption spectroscopy and X-ray diffraction of fuel cell electrocatalysts

Andrea E. Russell[a,*], Stephanie Maniguet[a], Rebecca J. Mathew[a], Jun Yao[a], Mark A. Roberts[b], David Thompsett[c]

[a]*Department of Chemistry, University of Southampton, Highfield, Southampton SO17 1BJ, UK*
[b]*CLRC, Daresbury Laboratory, Warrington, Cheshire WA4 4AD, UK*
[c]*Johnson Matthey Technology Centre, Blounts Court, Sonning Common, Reading RG4 9NH, UK*

Received 12 January 2001; accepted 14 January 2001

Abstract

The utility of in situ X-ray absorption spectroscopy (XAS) in determining structural parameters, through analysis of the extended X-ray absorption fine structure (EXAFS), and electronic perturbations, through a white line analysis of the X-ray absorption near edge structure (XANES), is demonstrated for Pt/C, PtRu/C and PtMo/C fuel cell electrodes. The results provide verification that the enhancement of CO tolerance of the alloy catalysts occurs via an intrinsic mechanism for the PtRu alloy, whilst a promotion mechanism is in operation for the PtMo alloy. Preliminary results of an in situ powder X-ray diffraction (XRD) method which utilises synchrotron radiation (SR) and a curved image plate detector are also presented, using Pd/C as an example. The lattice expansion upon formation of the β-hydride is clearly observed. © 2001 Elsevier Science B.V. All rights reserved.

Keywords: Fuel cell catalysts; X-ray absorption spectroscopy; X-ray diffraction

1. Introduction

In recent years there has been an increased interest in electricity generation using fuel cells for both stationary and mobile applications. In particular, following announcements by several automotive manufacturers [1,2], the research and development effort in the area of PEM (proton exchange membrane) fuel cells has intensified. Such cells either use H_2 or CH_3OH as the fuel and O_2 or air as the oxidant. The electrocatalysts are usually based on small Pt metal particles dispersed on a conductive supporting medium, often carbon.

In the case of the H_2 or PEM fuel cell, the source of the fuel is usually reformate, which is a mixture of H_2 and CO_2 obtained by processing (reforming) a hydrocarbon feed stock. Reformate produced by steam or partial oxidation, contains 0.5 to 2% CO. The CO contamination is then reduced to ppm levels prior to entering the fuel cell by clean up stages (selective oxidation). However, even at 10 ppm CO, a further reduction is required as, even at such levels, CO can cause deactivation of the anode catalyst by strongly adsorbing to the more active sites; a site blocking mechanism. Adding an air bleed to the anode fuel stream and performing the final CO clean up within the membrane electrode assembly (MEA) are the most generally applied approaches to improving CO tolerance. However, the more elegant alternative is to develop electrocatalysts that are 'tolerant' to the presence of CO in the fuel. The most promising electrocatalysts are now based on binary and ternary alloys of Pt. The ultimate performance of the H_2 fuel cell is also limited by the rate of the O_2 reduction reaction at the cathode.

As in the case of the electrocatalysts for the anode, alloys of Pt have been investigated in an effort to improve the performance of the cathode. In the case of the direct methanol fuel cell (DMFC), the anode catalyst may be slowly deactivated by the accumulation of partial oxidation products such as CO, while the cathode is depolarised by crossover of methanol from the anode side of the cell. Alloy electrocatalysts may also provide solutions to these difficulties.

Characterisation of the electrocatalyst materials is usually conducted ex situ using BET, TEM, or XRD measurements. Recently, with the increased availability of synchrotron radiation (SR), the use of in situ X-ray absorption spectroscopy (XAS) has been shown to be uniquely suited to

* Corresponding author. Fax: +44-1703-593781.
E-mail address: a.e.russell@soton.ac.uk (A.E. Russell).

0378-7753/01/$ – see front matter © 2001 Elsevier Science B.V. All rights reserved.
PII: S0378-7753(01)00573-0

determining the structure of such electrocatalysts. In situ XAS enables the probing of both the d-electronic structure of the metal particles (oxidation state and size/delocalization) and the interaction of these particles with their support and adsorbates (near neighbour interactions). The in situ study of carbon supported Pt (Pt/C) fuel cell electrodes was first successfully demonstrated by O'Grady and Koningsberger [3]. Mathew and Russell have recently presented a comprehensive review of the use of XAS for the characterisation of Pt/C, highlighting the development of the technique [4]. The most significant advances have been in the development of energy dispersive EXAFS (EDE) methods, which enable dynamic or time resolved studies of the catalyst structure.

In this paper the utility of in situ XAS methods in determining the structure of Pt/C, PtRu/C and PtMo/C catalysts is demonstrated. The results are related to the improvement in CO electro-oxidation for the binary catalysts over that of Pt/C. In addition, in situ X-ray diffraction (XRD) measurements using SR and a curved image plate camera is presented for the Pd/C system.

2. Experimental

2.1. Electrodes

An appropriate quantity of 40 wt.% Pt/XC-72R, or 40 wt.% Pt plus 20 wt.% Ru/XC-72R, or 35 wt.% Pt plus 5 wt.% Mo/XC72-R catalyst (supplied by Johnson Matthey, the preparation of which has been previously reported [5]) or 40 wt.% Pd/XC72-R (E-TEK) was suspended in Nafion® and water to form an ink-like paste. The paste was stirred for 15 min and then spread onto carbon paper (E-TEK TGHP-120). The sheet was pressed at 14 kg cm^{-2} for 20 s at room temperature. Electrodes of area 2.5 cm^2 were cut from the compressed sheet for the in situ EXAFS and XRD measurements and 1 cm^2 for cyclic voltammetric (CV) testing. Electrodes were boiled in triply distilled water prior to EXAFS and CV studies to ensure a fully flooded state.

2.2. Cyclic voltammetry

The wetted electrodes were placed in a standard three-electrode cell for the CV experiments. Potentials were measured either with respect to a Hg/Hg_2SO_4 (MMS) reference electrode or a H_2 purged Pd on carbon electrode strip acting as a reversible hydrogen electrode (RHE). When the MMS reference electrode was used the potentials have been corrected to the RHE scale.

For CO electro-oxidation experiments, the catalyst electrodes were held at 0.15 V versus RHE while CO and N_2 was purged through the electrolyte for 15 and then 30 min, respectively. The electrode potential was then cycled to the positive limit and back to 0.05 V at a sweep rate of 10 mV s^{-1}.

2.3. X-ray absorption spectroscopy measurements

The in situ transmission data was collected using a cell described previously [6]. The carbon paper backed catalyst working electrode was placed against a gold wire current collector and several layers of filter paper soaked in electrolyte, 1.0 mol dm^{-3} H_2SO_4 prepared with 18 MΩ cm water, were placed over the electrode. This assembly was compressed between Kapton® or polycarbonate windows, through which the X-rays passed.

All X-ray data were collected on Wiggler station 9.2 of the synchrotron radiation source (SRS) at Daresbury Laboratory, Warrington, England. The ring operated with 2.0 GeV energy and 100–250 mA current. The station was operated with a Si(2 2 0) double crystal monochromator, which was detuned to 50% intensity to minimise the presence of higher harmonics. Three ion chambers, optimised for the platinum L_{III} edge, were used in series to measure the intensities of the incident beam, I_o, the beam transmitted by the sample, I_t, and the beam subsequently transmitted by a platinum foil, I_m. The Pt foil was used as an internal reference, enabling calibration of the X-ray beam energy.

The absorption spectra were processed using EXBROOK. The zero point of the energy scale was taken to be the point of inflection in the L_{III} edge. The pre-edge region was fitted by a straight line and extrapolated to zero energy. A polynomial spline was fitted to the non-oscillatory component of the post-edge region and was extrapolated back to zero energy. The difference between the extrapolated values was taken to be the step height and the spectrum was normalised to this value. The EXAFS components, $\chi(k)$, were then isolated from the absorption spectra and subsequently analysed using EXCURV98 [7], a least squares fitting programme based on curved-wave theory, using a $Z + 1$ 2p core hole approximation.

2.4. X-ray diffraction measurements

The in situ XRD data was collected using a similar electrochemical cell to that used for the XAS measurements. On the exit side of the cell an enlarged slit was cut into the cell body and support to enable collection of the diffracted signal over a greater angular spread. The data was collected using Station 9.1 of the SRS. This station accepts a high energy X-ray spectrum of radiation from a 5 Tesla superconducting Wiggler. The monochromator was a Si(1 1 1) channel-cut crystal mounted at 15 m from the source and was used to select a wavelength, typically between 0.46 and 0.70 Å when using the Curved Image-Plate (CIP) camera [8]. This wavelength range is restricted because the high-energy flux is diminishing rapidly and the longer wavelength is a maximum at 0.70 Å since $\lambda/3$ harmonics become prominent and contaminate the data. A wavelength of 0.6920 Å was selected and calibrated using a Zr metal absorption foil. The monochromatised beam was reduced in size to 0.5 mm × 0.5 mm and this was passed down the

anti-scatter tube arrangement to impinge on the sample in the cell approximately 1 m from the monochromator. The sample was located at the centre of curvature of the 350 mm radius camera arc. Any positional discrepancy is corrected by collecting data from an NBS 640b silicon standard and spatial distortions introduced during the image-plate reading are corrected using a grid calibration. Utilising a significant proportion of the area of the image-plate it is possible to collect high quality data on materials over a few minutes.

The processed data were subsequently analysed by the Le Bail method using the program WinMProf. The Le Bail method is used to extract the intensities of the overlapping peaks from powder data without a structural model, given a starting set of unit cell parameters, and a list of possible reflections. Essentially, the method is similar to Rietveld in that a calculated profile is refined by least-squares against the observed diffraction pattern. Hence lattice parameters, peak widths, peak-shape parameters are allowed to vary. The same procedure was used for each data set.

3. Results and discussion

3.1. Cyclic voltammetry

Fig. 1 shows the cyclic voltammograms obtained for electro-oxidation of adsorbed carbon monoxide for each of the Pt and Pt-alloy catalyst electrodes. For each of the electrodes, during the first forward sweep (from 0.05 to 1.0 V) the peaks characteristic of hydrogen desorption were suppressed by the presence of adsorbed CO, indicating nearly full CO coverage. The peak at 0.8 V in the Pt/carbon CV corresponds to the oxidative stripping of the adsorbed CO layer. On the second sweep the voltammogram returns to that observed in the absence of CO purging and corresponds to that of Pt in the base electrolyte. Similar features are apparent in the PtRu/C and PtMo/carbon CVs with the peak potential of the CO oxidation shifting to 0.48 and 0.78 V, respectively. The lack of distinct hydrogen adsorption/desorption peaks in the PtRu/carbon CV is characteristic of the response of a PtRu alloy. On close inspection of the PtMo/carbon CV, an oxidation current is observed throughout the first forward sweep, from 0.15 to 1.00 V, suggesting that some of the adsorbed CO is being oxidised at lower potentials. An additional oxidation peak is observed in the second forward sweep at 0.45 V, which has previously been attributed redox reactions of the Mo on the surface of the metal particles [9]. These results have been discussed recently in terms of the heterogeneity of the PtMo/C electrocatalyst in comparison to PtRu/C [10].

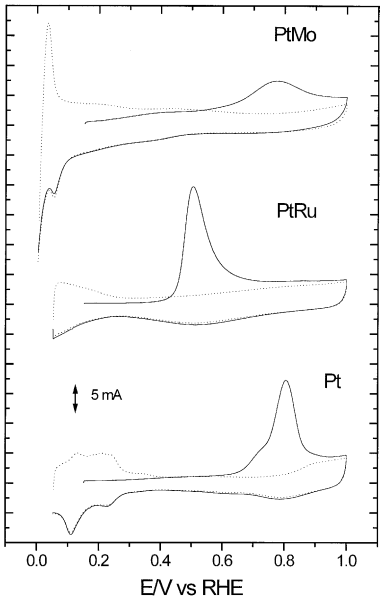

Fig. 1. Cyclic voltammograms of Pt/C, PtRu/C, and PtMo/C catalysts in 1 mol dm^{-3} H_2SO_4 at 10 mV s^{-1} (electrode area 1 cm^2). The electrode surface was exposed to CO saturated solution while the potential was held at 0.15 V vs. RHE. After adsorption, CO was displaced from the solution by purging with N_2 for 15 min. The solid lines represent the first cycle and the dashed lines the second.

3.2. X-ray absorption

The XANES (X-ray absorption near edge structure) or white line region of the Pt L_{III} and L_{II} absorption edges provides information regarding the d-electron occupancy of the metal particles. Comparisons of the area under the white lines of the sample and a Pt foil have been used previously [11–14] to quantify the changes in the relative occupancy, f_d, of the Pt as a function of the applied electrode potential. f_d is defined as follows [15]:

$$f_d = \left(\frac{\Delta A_3 + 1.11\Delta A_2}{A_{3r} + 1.11A_{2r}}\right) \quad (1)$$

where ΔA_3 is the difference in the area under the white line at the L_{III} absorption edge between the sample and the Pt reference foil ($\Delta A_3 = A_{3s} - A_{3r}$). Similarly $\Delta A_2 = A_{2s} - A_{2r}$, is the difference at the L_{ii} absorption edge. Thus, a smaller value of f_d indicates a greater occupancy of d electrons per Pt atom.

Fig. 2 shows the effect of variation of the applied electrode potential on the white line features at the Pt L_{III} and L_{II} absorption edges for the Pt/C sample. The effect of increasing the applied potential is to increase the area in the white line region, this corresponds to an increase in the f_d value. The f_d values as a function of the applied potential for the Pt and Pt-alloy catalysts are shown in Table 1. The effect of incorporation of the secondary metal is to decrease the d-electron occupancy per Pt atom (increased f_d) at the lower potentials. Thus, the electronic state of the Pt in the alloy catalysts at these potentials corresponds to a pre-oxidised state. As the potential is increased the f_d values of all the catalysts increases, but that of the alloy catalysts do not change as much as that of the Pt/C.

The k^1 weighted raw EXAFS data for the Pt/C electrode at 0.05 V is shown in Fig. 3. The corresponding k^3 weighted

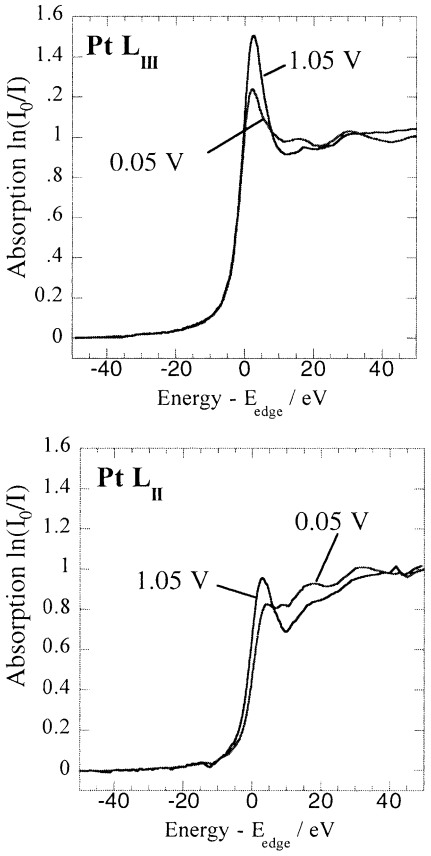

Fig. 2. XAS in 1 mol dm^{-3} H_2SO_4 showing the XANES region at the Pt L_{III} and L_{II} absorption edges for Pt/C at 0.05 and 1.05 V vs. RHE.

Table 1
Fractional d-electron occupancy, f_d, as a function of applied potential

E/*V* vs. RHE	Pt/C	PtRu/C	PtMo/C
0.05	−0.095	−0.029	−0.055
0.25	−0.002	−0.019	−0.024
0.55	0.024	0.000	0.012

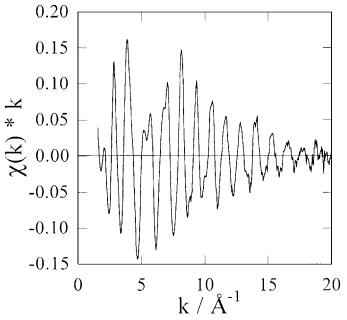

Fig. 3. k^1 weighted EXAFS at 0.05 V vs. RHE for Pt/C fuel cell electrode in 1 mol dm^{-3} H_2SO_4.

Pt–Pt phase corrected Fourier transform is shown in Fig. 4, with those for the PtRu/C and PtMo/C catalysts. The dashed lines indicate the best fit of the data. The splitting of the peak corresponding to the first coordination shell for the PtRu/C catalyst is caused by interference between the backscattering from Pt and Ru neighbours. The parameters for the fits of the EXAFS data are given in Table 2. The smaller coordination numbers and distances for the supported particles compared to those for a Pt foil, $N = 12$ and $R = 2.779$ Å, are consistent with the small size of the particles and other EXAFS studies ([4] and references contained therein). The smaller total number of neighbours in the first coordination shell ($N(\mathrm{Pt{-}Pt}) + N(\mathrm{Pt{-}X})$, where X = Mo or Ru) indicates that the particles are smaller than for the Pt/C sample, in agreement with TEM measurements of the particle sizes [10]. The fits indicate that the PtRu/C is a well mixed alloy with almost equal numbers of Pt and Ru in the first coordination shell, whilst the PtMo/C catalyst has very little Mo in the first coordination shell. For icosahedral or cuboctahedral particles less than 5 nm in diameter, the fraction of the Pt atoms which are on the surface is approximately 0.5. Thus, the PtMo/C sample may consist of a Pt core with less than a full monolayer of Mo on the surface, or it may represent a mixed system with less than the stoichiometric quantity of

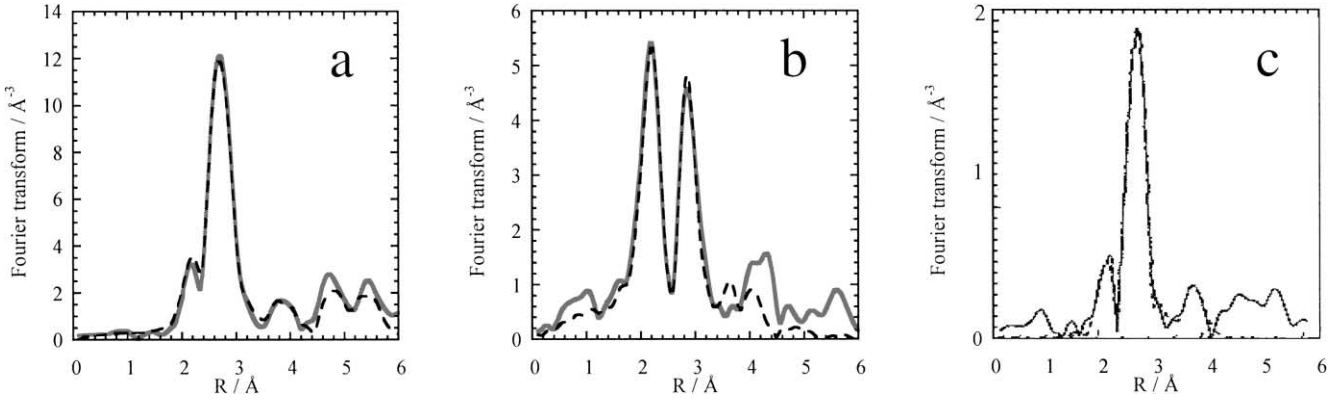

Fig. 4. k^3 weighted Pt–Pt phase corrected Fourier transforms of the data (solid lines) and model spectra (dashed lines) for the (a) Pt/C, (b) PtRu/C and (c) PtMo/C fuel cell electrodes at 0.05 V versus RHE in 1 mol dm^{-3} H_2SO_4.

Table 2
Fit parameters and variances for model spectra at 0.05 V vs. RHE[a]

Catalyst	Neighbour	N	R (Å)	$2\sigma^2$ (Å^2)
Pt/C	Pt–Pt	9.1	2.755	0.011
$R = 23\%$	Pt–Pt	4.4	3.912	0.016
	Pt–Pt	7.1	4.798	0.012
PtRu/C	Pt–Pt	4.4	2.732	0.011
$R = 25\%$	Pt–Ru	3.2	2.710	0.013
	Pt–Pt	1.9	3.850	0.017
PtMo/C	Pt–Pt	6.0	2.756	0.011
$R = 37\%$	Pt–Mo	0.3	2.431	0.014
	Pt–Pt	3.5	3.893	0.013

[a] Errors are ±10% in coordination number for the first Pt–Pt and Pt–X distances and ±50% for the higher shells, ±0.004 Å in coordination distance for the first and second Pt–Pt and Pt–X distances, and 0.003 for the Debye Waller term ($2\sigma^2$). The goodness of fit parameter, R, is $R_{\mathrm{EXAFS}} = \left\{\sum_i^N (1/\sigma_i^{\mathrm{exp}})(|\chi_i^{\mathrm{exp}} - \chi_i^{\mathrm{th}}|)\right\} \times 100\%$ where N is the total number of data points, σ the standard deviation for each data point, and χ the experimental and theoretical EXAFS.

Mo in the particle. EXAFS measurements obtained at the Mo edge are required to discriminate between these two possibilities.

Improvements in the tolerance of electrocatalysts to carbon monoxide exposure or methanol crossover upon alloy formation are thought to be related to either variations in the chemisorptive properties of the particles (intrinsic mechanism) or electronic effects which lead to a reduction in the activation overpotential (promotion mechanism). For PtRu/C the intrinsic mechanism is thought to dominate, whilst for PtMo/C the promotion mechanism is thought to be more important [16]. The in situ XAS results described above provide evidence supporting these conclusions.

The PtRu/C catalyst used in this study was shown to be a well mixed alloy, in contrast to those investigated by Rolison et al. [17]. In their work, using ex situ XPS analysis of as prepared PtRu/C materials (obtained from E-TEK), they showed that much of the Ru in such catalysts exists as a separate amorphous RuO_x phase. In conclusion, they proposed that these ruthenium oxides are beneficial in that they enhance the proton conductivity of the catalyst material. In a separate study we have obtained XAS data at both the Pt L_{III} and Ru K absorption edges for well mixed and poorly mixed PtRu/C catalysts [18]. Examination of the Ru EXAFS data verified that at the potentials at which H_2 oxidation occurs (for well mixed PtRu/C catalysts) the Ru is metallic in nature. In fact, Cooper et al. [19], have shown that the oxidation of 100% CO on well alloyed PtRu/C does not occur at a significant rate below 0.2 V versus RHE. The EXAFS results also show a significant contraction in the Pt–Pt distance for the PtRu/C as compared to the Pt/C sample. This contraction, along with the electronic effect of alloying with Ru on the Pt atoms in the particles, is likely to result in a modification of the chemisorptive behaviour of CO on the Pt sites. We have recently shown that EXAFS is a useful probe for the investigation of the bonding of CO to Pt in Pt/C catalysts [6]. Further EXAFS investigations of the effect of Ru on the bonding of CO to the Pt sites are underway.

The PtMo/C catalyst used in this investigation was not shown to be a well mixed alloy system. In fact, the small number of Mo atoms in the first coordination shell and the lack of a significant variation in the Pt–Pt coordination distance, indicate that it is likely that the Mo is situated on the surface of the Pt particles. Preliminary analysis of the Mo K edge XAS data of an E-TEK PtMo/C catalyst has recently been reported by Mukerjee et al. [20]. They showed that that the Mo exists as $Mo(OH)_2^{2+}$ at 0.0 V and that the oxidation state of the Mo is potential dependent. The electronic effect of the addition of Mo on the Pt atoms in the particles is much weaker than that observed for the PtRu/C (see Table 1). The promotion of the oxidation of chemisorbed CO at low potentials, <0.1 V versus RHE, upon the addition of Mo is thus attributed to the formation of oxy-hydroxide species at the Mo sites rather than a change in the Pt–CO bond.

Ex situ XRD is commonly used to determine the extent of intermixing in alloy catalysts. The lattice constants obtained for fcc crystallites, such as Pt/C, may be compared with the second Pt–Pt distance in the model of the EXAFS data. However, XRD only probes the crystalline portion of the sample, whilst EXAFS probes the entire sample. In fact, we have obtained very different EXAFS results for several PtRu/C catalysts which all had similar lattice constants as determined by XRD [18]. In addition, the EXAFS data may be collected in situ, under electrochemical control. To enable more realistic comparison between XRD and EXAFS studies, we have sought to develop an in situ XRD method.

3.3. In situ X-ray diffraction

The Pd/C system was chosen as a first illustrative example, as the lattice is known to expand at potentials where hydrogen is incorporated. Cyclic voltammograms of the Pd/C electrode in 1 mol dm^{-3} H_2SO_4 are shown in Fig. 5. The large peaks observed in the first cycle from 0.05 to 0.45 V are attributed to desorption of adsorbed hydrogen incorporated into the Pd lattice when the potential is held below 0.05 V. The XRD patterns obtained using the CIP detector as a function of the applied potential for the Pd/C electrode are shown in Fig. 6.

The lattice constants obtained are summarised in Table 3. The lattice constants obtained may be compared with those of bulk Pd metal, 3.8900 Å [21], and the β-hydride ($PdH_{0.56}$), 4.018 Å [22]. The lattice constants obtained at 0.55 and 0.15 V are both slightly larger than that obtained for Pd metal, but show little effect of adsorbing H (at 0.15 V). That at −0.05 V, where H is absorbed, is also larger than that of the bulk β-hydride. The differences may represent a systematic error, caused by imprecise positioning of the electrochemical cell at the focus of the CIP. However, these preliminary results do demonstrate the utility of the in situ XRD method using the CIP.

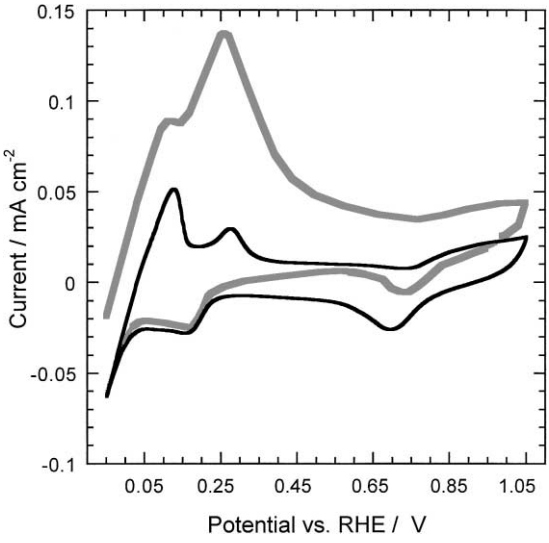

Fig. 5. Cyclic voltammogram of Pd/C fuel cell electrode (electrode area 1 cm^2) in 1 mol dm^{-3} H_2SO_4 at 20 mV s^{-1}. Grey line shows the first cycle after the potential was held at −0.05 V vs. RHE for 10 min, black line shows the fourth cycle.

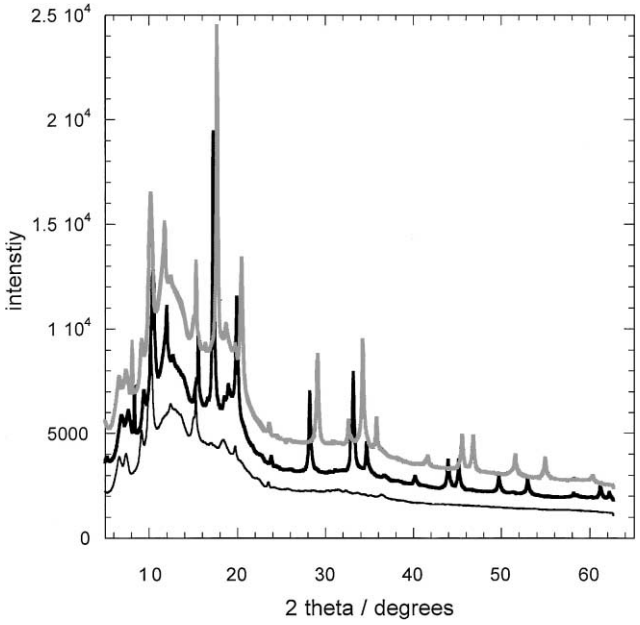

Fig. 6. XRD patterns for empty electrochemical cell (thin black line), Pd/C electrode at 0.15 V vs. RHE in 1 mol dm^{-3} H_2SO_4 (thick grey line) and at −0.05 V vs. RHE (thick black line). Data were collected using a curved image plate detector with 20 min exposures.

Table 3
Lattice parameters and standard deviations for Pd/C as a function of applied electrode potential

E vs. RHE (V)	Lattice parameter (Å)	ESD (Å)
0.55	3.8957	0.0008
0.15	3.8955	0.0010
−0.05	4.0504	0.0010

4. Summary

The increased availability of SR has enabled the use of in situ XAS to become more routine in the investigation of carbon supported catalysts used in PEM fuel cells. For the examples described in this paper, Pt/C, PtRu/C, and PtMo/C, the information obtained from analysis of the white line or near edge and EXAFS regions of the XAS has added weight to the assertion that the mechanisms by which Ru and Mo increase the CO tolerance of Pt/C catalysts are different. Ru promotion occurring by the intrinsic mechanism is thought to dominate, whilst Mo acts via the promotion mechanism. Finally, preliminary results describing an in situ XRD method based on SR and the curved image plate detector were presented.

Acknowledgements

The authors would like to thank Johnson Matthey for the loan of the electrocatalyst materials and Fred Mosselmans and Chris Corrigan (Darebury Laboratory) for their assistance while at the SRS. RJM and JY acknowledge the support of the EPSRC through Quota studentships. The project is jointly supported by the EPSRC (GR/L69817), DERA through the Joint Grants Scheme, and Johnson Matthey.

References

[1] http://www.daimlerchrysler.de/index_e.htm?/news/top/t90317_e.htm; Daimler Chrysler Necar announcement.
[2] http://www.hfcletter.com/letter/march98/feature.html; GM PEM Fuel cell car to be launched with its European subsidiary, Opel.
[3] W.E. O'Grady, D.C. Koningsberger, Electrochem. Soc. Extended Abstr. 88 (1) (1988) 513.
[4] R.J. Mathew, A.E. Russell, Topics Catal. 10 (2000) 231.
[5] L. Keck, H. Buchanan, G Hards, US Patent, 5,068,161 (1991).
[6] S. Maniguet, R.J. Mathew, A.E. Russell, J. Phys. Chem. B 104 (2000) 1998.
[7] M.A. Roberts, J.L. Finney, G. Bushnell-Wye, Mater. Sci. Forum 278 (1998) 318.
[8] N. Binstead, EXCURV98: CCLRC Daresbury Laboratory computer program (1998).
[9] B.N. Grgur, N.M. Markovic, P.N. Ross, Electrochem. Soc. Proc. 98 (27) (1998) 176.
[10] S.C. Ball, A. Hodgkinson, G. Hoogers, S. Maniguet, D. Thompsett, B. Wong, Electrochem. Solid State Lett., submitted for publication.
[11] H. Yoshitake, T. Mochizuki, O. Yamazaki, K.-I. Ota, J. Electroanal. Chem. 361 (1993) 229.
[12] H. Yositake, O. Yamazaki, K.-I. Ota, J. Electroanal. Chem. 371 (1994) 287.
[13] H. Yoshitake, O. Yamazaki, K.-I. Ota, J. Electrochem. Soc. 141 (1994) 2516.
[14] S. Mukerjee, J. McBreen, J. Electroanal. Chem. 448 (1998) 163.
[15] A.N. Mansour, J.W. Cook Jr., D.E. Sayers, J. Phys. Chem. 88 (1984) 2230.
[16] G. Hoogers, D. Thompsett, Cattech. 3 (2000) 106.

[17] D.R. Rolison, P.L. Hagans, K.E. Swider, J.W. Long, Langmuir 15 (1999) 774.
[18] S. Maniguet, R. Mathew, J. Yao, D. Thompsett, A.E. Russell, unpublished results.
[19] S.J. Cooper, A.G. Gunner, G. Hoogers, D. Thompsett, in: Proceedings of the 2nd International Symposium on New Materials for Fuel Cells and Modern Battery Systems, Montreal, Quebec, Canada, 1997.
[20] S. Mukerjee, S.J. Lee, E.A. Ticianelli, J. McBreen, B.N. Grgur, N.M. Markovic, P.N. Ross, J.R. Giallombardo, E.S. De Castro, Electrochem. Solid State Lett. 2 (1999) 12.
[21] D.W. Murphy, S.M. Zahurak, B. Vyas, M. Thomas, M.E. Badding, W.-C. Fang, Chem. Mater. 5 (1993) 767.
[22] A.F. Wells, Structural Inorganic Chemistry, 5th Edition, Clarendon Press, Oxford, 1984.